Preprint

Piezo1-mediated spontaneous activity of satellite glia impacts DRG development

Jacob P. Brandt[1,2] and Cody J. Smith[1,2]*

1 Department of Biological Sciences, 2 The Center for Stem Cells and Regenerative Medicine[2] at the University of Notre Dame, Notre Dame, IN.

*Cody J. Smith, csmith67@nd.edu

ABSTRACT:
Spontaneous activity of neural cells is a hallmark of the developing nervous system. It is widely accepted that chemical signals, like neurotransmitters, contribute to spontaneous activity in the nervous system. Here we reveal an additional mechanism of spontaneous activity that is mechanosensitive in the peripheral nervous system using intravital imaging of growing dorsal root ganglia (DRG) in zebrafish embryos. GCaMP6s imaging shows that developing DRG glia contain distinct spontaneous Ca^{2+} transients, classified into simultaneous, isolated and microdomains. Longitudinal analysis over days in development demonstrates that as DRG glia become more synchronized, isolated activity remains constant. Using a chemical screen, we identify that Ca^{2+} transients in DRG glia are dependent on mechanical properties, which we confirmed using an experimental application of mechanical force. We find that isolated spontaneous activity of the glia during development is altered by manipulation of mechanosensitive protein Piezo1, which is expressed in the developing ganglia. In contrast, simultaneous activity of DRG glia is not Piezo1-mediated, thus demonstrating that distinct mechanisms mediate subtypes of spontaneous activity. Activating Piezo1 eventually impacts the cell abundance of DRG cells and behaviors that are driven by DRG neurons. Together, our results reveal mechanistically distinct subtypes of Ca^{2+} transients in satellite glia and introduce mechanobiology as a critical component of spontaneous activity in the developing peripheral nervous system.

INTRODUCTION:
It is widely accepted that spontaneous activity is a critical feature of the developing nervous system[1–3]. For years, such spontaneous activity has been investigated in neurons, but recent studies have also revealed an important role for spontaneous activity in glia. This glial activity can be in response to neuronal activity or independent of neuronal activity and can be characterized into distinct subtypes[4–7]. For example, glial cells exhibit whole cell and microdomain Ca^{2+} transients, which are mechanistically and functionally distinct[8–10]. Glial cells can also exhibit synchronous Ca^{2+} transients in physically-connected networks[11,12]. Regardless of Ca^{2+} transient subtype and unique from neurons, glia and their progenitors also proliferate throughout life[13]. How glial activity, proliferation and physically-connected networks are related or regulated, remains largely unexplored. The importance of these concepts is underscored by the prevalence of such processes during normal brain development and in gliomas[4,5,14–16]. If glial Ca^{2+} transients are critical for nervous system function, we need more investigation into how distinct Ca^{2+} transients change over development, whether different molecular components control distinct transient subtypes, and if distinct Ca^{2+} transients are linked to proliferation and/or network formation. Lastly, these concepts need to be explored in both the CNS and PNS.

What we do know is that spontaneous activity in the nervous system has largely been characterized to be dependent on chemical signals. In neurons, spontaneous activity is promoted by neurotransmitters and their receptors[17,18]. Similarly, glutamate and NMDA drive spontaneous activity of glial cells like oligodendrocytes and astrocytes[19–22]. We also know chemical signals like ATP can induce purinergic receptors to drive Ca^{2+} changes in glia, akin to activity of the glia[23–25]. Each of these chemical signals causes changes to ion channels that drive spontaneous activity. However, in addition to ion channels that are induced by chemical signals, mechanosensitive ion channels are also present in the nervous system[26,27]. For example, Piezo proteins are mechanosensitive channels that are expressed in the nervous system[26,28,29]. These mechanosensitive channels are essential for evoking a subset of peripheral sensory neurons in response to mechanical stimulation[30,31]. Peripheral mechanosensitive glia are also present at the skin to ensure response to mechanical stimuli[32]. However, the role of mechanosensitive properties in the development of glia is less understood, especially in peripheral glia. This is despite knowledge that mechanical components can have profound effects on cell differentiation and tissue organization and that Trp channels, some of which are at least partially mechanosensitive, are important for Ca^{2+} transients in glia like astrocytes[4,8,29,33–36].

Here we use imaging of GCaMP6s in non-neuronal and progenitor cells of the DRG in zebrafish as a model to investigate the role of glial activity in the developing peripheral nervous system. The DRG is required for somatosensory stimuli in the PNS and contains somatosensory neurons and satellite glia that ensheath those neurons. We identify that satellite glia display at least three types (microdomain, isolated, and simultaneous) of spontaneous Ca^{2+} transients in early phases of development. By mapping the GCaMP6s events, we identify that the DRG transitioned to synchronized activity early in development, demonstrating the formation of glial networks within the first three days of DRG construction. In a pilot screen and follow-up experimental manipulations, we identify mechanosensitive ion channel Piezo1 as a modulator of the isolated activity of non-neuronal cells in development and identify that these non-

neuronal cells are mechanosensitive. Perturbation of Piezo1 causes not only changes in isolated activity of DRG cells but also in their expansion and function, demonstrating a potential consequence to altering isolated glial activity during development. Together, we introduce the role of mechanosensitive ion channels in the spontaneous activity of the developing peripheral nervous system.

RESULTS:

DRG non-neuronal cells exhibit distinct Ca^{2+} transients

To understand if DRG glia display spontaneous activity, we first explored the activity of DRG cells in intact ganglia using intravital imaging in zebrafish. To do this we imaged transgenic animals expressing GCaMP6s in distinct DRG cell populations. To image glia and other non-neuronal cells, including satellite glia, we labeled the population using *Tg(sox10:gal4+myl7); Tg(uas:GCaMP6s); Tg(neurod:tagRFP)* animals, allowing us to determine the changes in GCaMP6s in non-neuronal ($tagRFP^-$) cells. We also imaged neurons in the DRG using *Tg(neurod:gal4+myl7); Tg(uas:GCaMP6s)*, which uses regulatory sequences of *neurod* that are expressed in DRG neurons. We imaged these animals at a 15 second interval for 1 hour, which allowed us to capture a three-dimensional view of 3-4 DRG. To define a cell activity event, we calculated the z score of the integrated density of fluorescence of each individual cell during that 1-hour time period. Time points with a z score greater than 2.58 (represents 99% confidence interval) were considered active time points. Scoring of the z score of GCaMP6s integral density of fluorescence over the 1 hour period revealed that all DRG displayed cells with spontaneous activity, with remarkable activity in non-neuronal cells (Fig 1A,B). Within individual DRG, glia displayed on average 3.600±1.78 Ca^{2+} activity events in a 1-hour period (Sup Fig 1A). We also measured 2.364±1.12 Ca^{2+} activity events in the neuronal population in a 1-hour period (Sup Fig 1A), indicating that both neurons and glia are active during DRG construction. Ca^{2+} transients can be quick in cells, so it is possible that a 15 sec imaging interval under-represented the number of Ca^{2+} transients. To address this, we imaged smaller z-stacks but with short time intervals of 5 secs. These results revealed that Ca^{2+} transients in *sox10*$^+$ cells lasted on average 2.21 timepoints using 5 sec imaging intervals and therefore were generally captured with 15 sec intervals (Sup Fig 1B). We therefore utilized 15 sec imaging intervals throughout this manuscript, allowing us to image z-stacks that covered the entire DRG at each timepoint. With the lack of knowledge about glial activity in the DRG, we further investigated the developmental, molecular, and functional features of Ca^{2+} transients in *sox10*$^+$ cells.

Neural cells can exhibit distinct spontaneous Ca^{2+} events. To explore if DRG non-neuronal cells exhibit distinct subtypes of Ca^{2+} transients, we created activity profiles for each cell in a given DRG from z-score calculations in 1 hour movies of *Tg(sox10:gal4+myl7); Tg(uas:GCaMP6s); Tg(neurod:tagRFP)* animals. Using this data, we could then compare when each individual cell in a DRG was active compared to the other cells in the DRG. We found that individual *sox10*$^+$ cells were active while other cells in the DRG were active (Fig 1E), consistent with previous descriptions of simultaneous activity in glial networks. However, we also identified a subset of Ca^{2+} transients that occurred in cells when no neighboring cell is active (Fig 1E). We define this activity in this report as isolated activity.

Calcium microdomains are also known to be present in several glial types[10,34,37]. Therefore, we tested if Ca^{2+} microdomains are also present in the DRG during development. To do this, we imaged animals expressing a membrane localized GCaMP6s by injecting *Tg(sox10:gal4+myl7)* embryos with *uas:GCaMP6s-caax* and imaging at 3 dpf. In order to initially capture and identify these quick dynamic events we imaged animals for a 10 minute period with 5 second intervals capturing the entire DRG. We defined Ca^{2+} microdomains as small regions with significant changes in integrated density of fluorescence of GCaMP6s-caax (Fig 1C,D). Together, these results indicate non-neuronal DRG cells exhibit at least three distinct Ca^{2+} events during development: isolated, simultaneous, and microdomains.

Non-neuronal cell networks are established during early DRG construction

To understand how these types of activity may change over development, we quantified the average amount of isolated and simultaneous activity-types in the same animal at 2, 3, and 4 dpf. While we did not see a significant change in isolated activity over this developmental period (Fig 1F), there was a noted increase in the number of simultaneous activity events after 2 dpf (2dpf vs. 3dpf: p=0.0019, 2dpf vs. 4dpf: p=0.0449 post hoc tukey test) (Fig 1G). This work indicates distinct developmental properties between isolated and simultaneous subtypes.

Current research proposes that DRG glia form networks *in vitro*[38–40]. To further test if this occurs *in vivo* and to determine when in development it arises, we measured synchronized networks in *sox10*$^+$ cells. To identify a synchronized network of cells we compared the activity profiles of individual cells by computing the correlation between two activity profiles. To determine how this changed in development, we quantified the percent of high correlation coefficients (<0.5) per cell in each DRG at 2, 3, and 4 dpf. By creating network maps of individual DRG that show how the activity of each cell is related (Fig 1H-I), we found that *sox10*$^+$ cells at 2 dpf had an average of 37.48%±32.08% high correlation coefficients. At 3 dpf we measured that *sox10*$^+$ cells had an average of 39.33%±30.61% high correlation coefficients and by 4 dpf, *sox10*$^+$ cells had a significant increase in the percent of high correlation coefficients, with an average of 58.26%±32.13% high correlation coefficients (2dpf vs. 4dpf: p=0.0044 post hoc tukey test, 2dpf n=46 cells, 3dpf n=27 cells, 4dpf n=34 cells) (Fig 1J). Additionally, we observed that the percent of cells active together increased by 4 dpf (Sup Fig2A-C). These data are consistent with the hypothesis that DRG glial networks are present *in vivo* and form by at least the third day of DRG construction in zebrafish.

If glial networks are forming, we hypothesized that gap junctions may also increase during the time when synchronized Ca^{2+} activity is present. Cxn43 is known to be present in DRG and contribute to gap junctions in synchronized neural networks[41–43]. Therefore, we stained for Cxn43 at 2, 3, and 4 dpf in animals expressing *Tg(sox10:meGFP)*, which labels non-neuronal cells in the DRG with membrane-localized GFP. The 2 dpf DRG had an average of 0.500±0.707 Cxn43 puncta. This increased to an

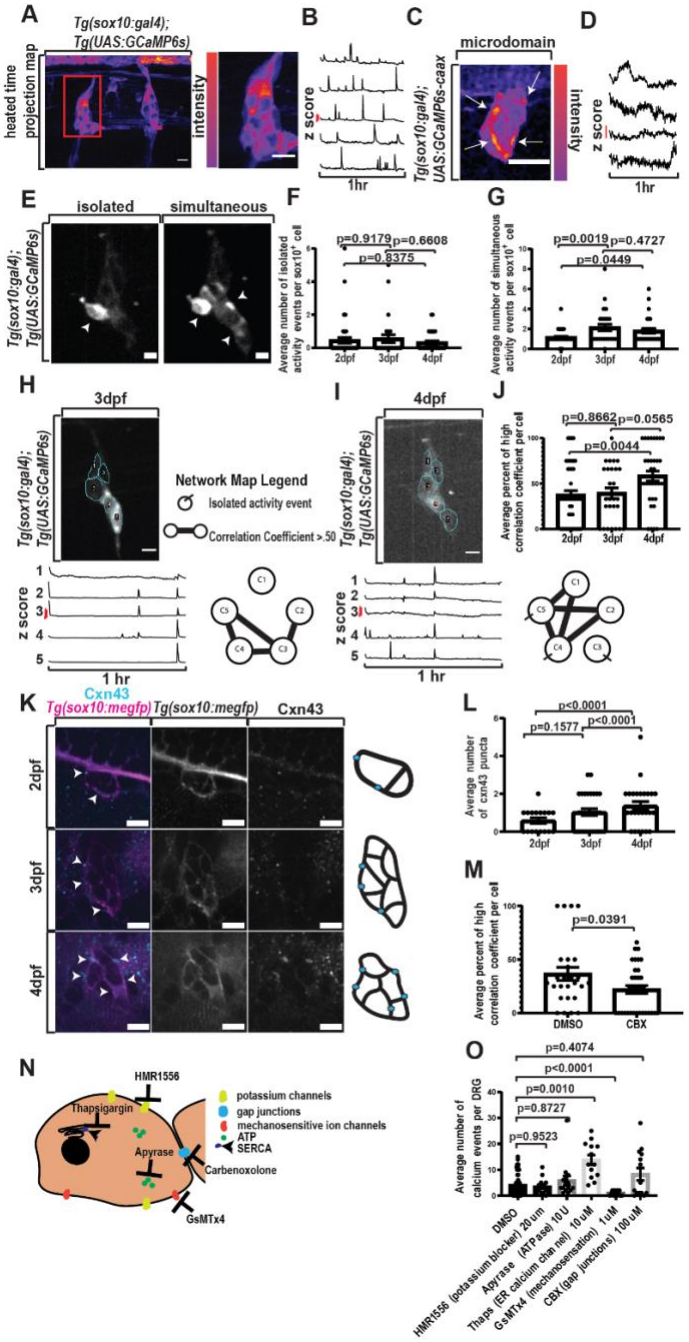

Figure 1: DRG exhibit distinct calcium activity and increase synchronous activity A) Confocal z-projections of DRG in a 3 dpf animal expressing *Tg(sox10:gal4);Tg(uas:GCaMP6s)*. Images presented as heated scale (reds-more activity, blues-less activity). B) Line graphs depicting z scores of integrated density of fluorescence for individual cells expressing *Tg(sox10:gal4); Tg(uas:GCaMP6s)*. A z score greater than 2.58 indicates an active Ca^{2+} event. Red scale bar is a z score of 2.58. C) Confocal z-projection of DRG in 3 dpf animal expressing *Tg(sox10:gal4); uas:GCaMP6s-caax*. Red colors indicate a higher intensity of fluorescence, and blue colors indicate a lower intensity of fluorescence. Arrows indicate active Ca^{2+} microdomains. D) Line graphs depicting z scores of integrated density of fluorescence for Ca^{2+} microdomains in 3dpf animals expressing *Tg(sox10:gal4); uas:GCaMP6s-caax*. A z score greater than 2.58 indicates an active Ca^{2+} event. Red scale bar is a z score of 2.58. E) Confocal z-projection of DRG in a 3 dpf animal expressing *Tg(sox10:gal4); Tg(uas:GCaMP6s)*. Left image depicts an isolated Ca^{2+} event, and the right image depicts a simultaneous Ca^{2+} event. Arrows indicate active cells. F) Average number of isolated Ca^{2+} activity events per *sox10*$^{+}$ cell at 2, 3, and 4 dpf in animals expressing *Tg(sox10:gal4); Tg(uas:GCaMP6s)*. G) Average number of simultaneous Ca^{2+} activity events per *sox10*$^{+}$ cell at 2, 3, and 4 dpf in animals expressing *Tg(sox10:gal4); Tg(uas:GCaMP6s)*. H-I) 3 (H) and 4 (I) dpf DRG in an animal expressing *Tg(sox10:gal4); Tg(uas:GCaMP6s)*. ROIs are traced for individual cells. A corresponding network map indicates both the number of isolated Ca^{2+} activity events and the high correlation coefficients present in the DRG. J) Percent of high correlation coefficient per *sox10*$^{+}$ cell in animals expressing *Tg(sox10:gal4); Tg(uas:GCaMP6s)* at 2, 3, 4 dpf. K) Immunohistochemistry for Cxn43 in DRG of animals expressing *Tg(sox10:meGFP)* at 2, 3, 4 dpf. Magenta indicates *Tg(sox10:meGFP)* and cyan indicates Cxn43. L) Quantification of the average number of Cxn43 puncta present in DRG at 2, 3, and 4 dpf. M) Quantification of the average percent of high correlation coefficients per *sox10*$^{+}$ cell following treatment with DMSO or CBX. N) Depiction of targeted cellular processes for molecular screen. O) Quantification of the average number of Ca^{2+} events per DRG following pharmacological screen. Scale bar is 10µm (A,C,E,H,I,K). Ca^{2+} activity events are timepoints containing a z score of the integrated density of fluorescence greater than 2.58 (B,D,F,G,H,I,J,M). Statistical tests: One-way ANOVA followed and represented by post hoc tukey test: (F,G,J,L), Unpaired student t tests: (M), One-way Brown-Forsythe ANOVA followed and represented by post hoc dunnett test: (O), Correlation coefficient test: (H,I,J,M).

average of 1.000±0.845 Cxn43 puncta per DRG at 3 dpf and by 4 dpf, there was a significant increase in the number of Cxn43 puncta present in the DRG with an average of 2.208±1.062 Cxn43 puncta per DRG (2dpf vs. 4dpf: $p<0.0001$, 3dpf vs 4dpf: $p<0.0001$ post hoc tukey test, 2dpf n=18 DRG, 3dpf n=29 DRG,4dpf n=24 DRG) (Fig 1K, 1L). These results support the hypothesis that DRG cells begin forming glial connections during its earliest construction.

To determine if there are functional gap junction connections, we treated animals expressing *Tg(sox10:gal4+myl7); Tg(uas:GCaMP6s); Tg(neurod:tagRFP)* with either Carbenoxolone (CBX), a gap junction inhibitor, or a control treatment of DMSO. Animals treated with CBX at 3 dpf demonstrated a significant decrease in the percent of high correlation coefficients with an average percent of 22.00%±22.34% compared to an average percent of high correlation coefficients of 36.58%±31.22% when treated with a DMSO control (CBX n=34 cells, DMSO n=26 cells, DMSO vs. CBX: $p=0.0391$ unpaired t test) (Fig 1M). These results strongly support the idea that functional gap junctions are present in glial networks in DRG during its early construction.

Non-neuronal Ca^{2+} transients are impacted by altering mechanobiology

Our measurements indicated that DRG non-neuronal cells demonstrate distinct Ca^{2+} transients. To identify potential molecular components involved in these Ca^{2+} transients, we performed a chemical screen targeting various chemical signals shown to affect Ca^{2+} activity using transgenic animals expressing

Tg(sox10:gal4+myl7); Tg(uas:GCaMP6s); Tg(neurod:tagRFP) (Fig 1N-O). Additionally, we included a broad-mechanosensitive ion channel antagonist, GsMTx4, because of the underappreciated role that mechanobiology has during neurodevelopment. We hypothesized that GsMTx4 would reduce the amount of observed Ca^{2+} activity if mechanobiology had an important role during early development. Each animal was exposed to the pharmacological agent 30 minutes prior and during the imaging window and then GCaMP6s intensity was measured for 1 hour with a 15s imaging interval. We reasoned that an overall change in the abundance of Ca^{2+} transients could help us identify molecules that are important for either isolated or synchronous spontaneous activity. We found that GsMTx4 significantly reduced the amount of Ca^{2+} activity observed compared to DMSO (Fig 1O) (DMSO vs. GsMTx4: p<0.0001 post hoc Dunnett test). We also measured a significant change following treatment with Thapsigargin (Thaps) (Fig 1O) (DMSO vs. Thaps: p=0.0010 post hoc Dunnett test). While chemical signaling has been widely described in spontaneous activity, the role of mechanobiology in the process is less known, which led us to investigate the potential role of mechanobiology in spontaneous activity in the DRG.

To first explore the possibility that mechanical features impact spontaneous activity in the DRG, we tested if the cells in the developing DRG are sensitive to mechanical perturbation. To do this, we imaged the DRG of transgenic zebrafish expressing GCaMP6s in non-neuronal *Tg(sox10:gal4+myl7); Tg(uas:GCaMP6s)* cells during tissue compression (Fig 2A). Tissue compression was administered by bending the animal with a microneedle as they were imaged on the confocal microscope (Fig 2B). At 2 dpf, 57% of DRG expressing

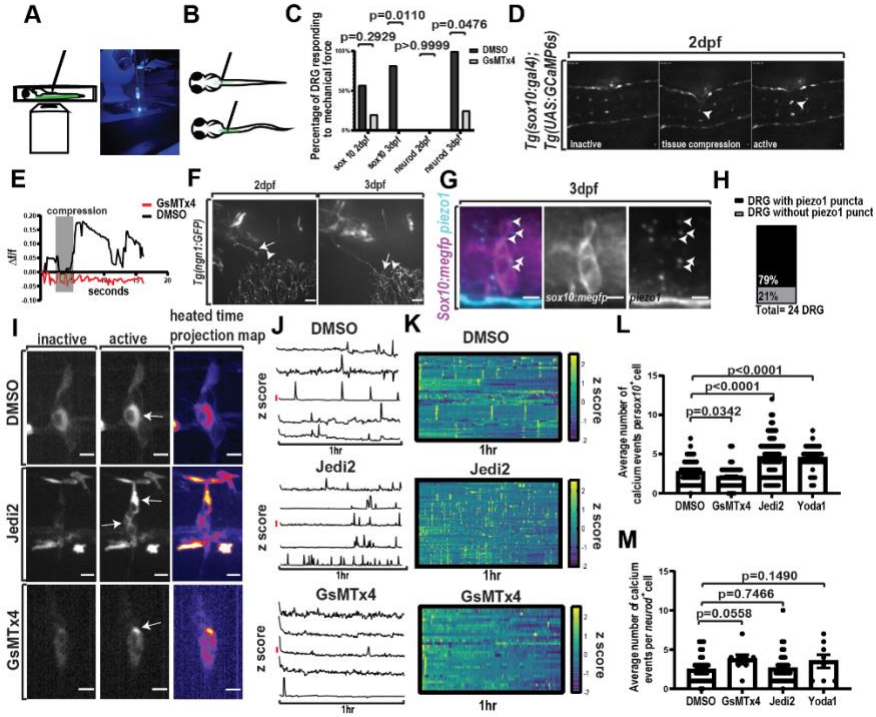

Figure 2: DRG are mechanosensitive and express *piezo1* A) LEFT Depiction of mechanical compression assay where animal is mounted dorsally on inverted spinning disk confocal with a dextran loaded microneedle mounted above the animal. RIGHT image of mechanical compression assay apparatus. B) Depiction of mechanical compression assay with needle placing force on DRG. C) Quantification of the percent of DRG responding to mechanical force in animals expressing *Tg(sox10:gal4); Tg(uas:GCaMP6s)* (labeled sox10) or expressing *Tg(neurod:gal4); Tg(uas:GCaMP6s)* (labeled neurod) and treated with either DMSO or GsMTx4 at both 2 and 3 dpf. D) Confocal image taken of the mechanical compression assay in 2 dpf animal expressing *Tg(sox10:gal4); Tg(uas:GCaMP6s)*. Images show an inactive time point, a time point with tissue compression, and an active time point in response to tissue compression. Inactive and active DRG marked with an arrow. E) Quantification of the change in integrated density of fluorescence of a DRG in a 2 dpf animal treated with either DMSO or GsMTx4. Change in integrated density of fluorescence is scored as time point subtracting the initial timepoint divided by time point $(\Delta f/f)$. Grey box notes timepoints of tissue compression. F) Confocal z-projection of peripheral DRG axon in an animal expressing *Tg(ngn1:GFP)* at 2 and 3 dpf. Arrow notes the end processes of the peripheral axon. Arrowhead denotes peripheral axons from Rohon beard neurons. G) Confocal images of RNAscope-*piezo1* and Immunohistochemistry-GFP in *Tg(sox10:meGFP)* animals. GFP is shown in magenta and *piezo1* is shown in cyan. Arrowheads indicate *piezo1* puncta. H) Quantification of DRG at 3 dpf with *piezo1* puncta and without *piezo1* puncta. I) Confocal images of 3 dpf animals expressing *Tg(sox10:gal4); Tg(uas:GCaMP6s)*. Red colors indicate a higher intensity of fluorescence, and blue colors indicate a lower intensity of fluorescence. Images depicted are of animals either treated with 2% DMSO, 40μM Jedi2, or 1μM GsMTx4. Arrows note active cells. H) Line graphs of z score of integrated density of fluorescence for a 1hr time period in 3 dpf animals expressing *Tg(sox10:gal4); Tg(uas:GCaMP6s)* that were treated with either 2% DMSO, 40μM Jedi2, or 1μM GsMTx4. A z score greater than 2.58 indicates an active Ca^{2+} event. Red scale bar shows a z score of 2.58. I) Heatmaps of the z score of individual *sox10*$^+$ cells from animals in G-H during a 1 hr period of Ca^{2+} imaging. Yellow notes a high z score (2.58 or greater). L) Quantification of the average number of Ca^{2+} events per *sox10*$^+$ cell in animals treated with either 2% DMSO, 1μM GsMTx4, 100μM Yoda1, or 40μM Jedi2. M) Quantification of the average number of Ca^{2+} events per *neurod*$^+$ cell in 3 dpf animals expressing *Tg(neurod:gal4); Tg(uas:GCaMP6s)* that were treated with either 2% DMSO, 1μM GsMTx4, 40μM Jedi2, or 100μM Yoda1. Scale bar 10μm (D,F,G,I). Statistical tests: unpaired t test (L, M), Fisher's exact (C).

Tg(sox10:gal4+myl7); Tg(uas:GCaMP6s) responded to tissue compression (Fig 2C-D). It is possible that this response of *sox10*$^{+}$ cells was secondary to neuronal firing. We, therefore, tested if neurons fired in response to compression at 2 dpf in *Tg(neurod:gal4+myl7); Tg(uas:GCaMP6s)* animals but could not detect Ca^{2+} transients in neurons after compression (Fig 2C). Scoring DRG axonal projections in *Tg(ngn1:GFP)* animals also showed that neurons at 2 dpf did not have peripheral axons at their final targets in the periphery. It therefore seems unlikely that such Ca^{2+} transients in *sox10*$^{+}$ cells after tissue compression are secondary to neuronal activity. To understand if *sox10*$^{+}$ cells continued to be sensitive to mechanical compression, we repeated this assay at 3 dpf. By 3 dpf, 82% (n=11 DRG) of DRG expressing *Tg(sox10:gal4+myl7); Tg(uas:GCaMP6s)* responded to tissue compression (Fig2C). At 3 dpf, 100% (n=5 DRG) of DRG expressing *Tg(neurod:gal4+myl7); Tg(uas:GCaMP6s)* also demonstrated Ca^{2+} transients after tissue compression (Fig 2C). While the neuronal population of the DRG does respond to activity at a later age, our data suggests glia respond to the mechanical tissue compression at early ages without neuronal activation.

If this response to mechanical force is mediated by mechanosensitive ion channels, we would hypothesize that it would be reduced upon treatment of GsMTx4, which broadly blocks mechanosensitive ion channels. To test this hypothesis, we imaged animals expressing either *Tg(sox10:gal4+myl7); Tg(uas:GCaMP6s); Tg(neurod:tagRFP)* or *Tg(neurod:gal4+myl7); Tg(uas:GCaMP6s)* that were treated with GsMTx4. We found that treatment with GsMTx4 reduced the response to mechanical stimuli to 20% of animals (n=5 animals) expressing non-neuronal GCaMP6s at 2 dpf (Fig 2C). At 3 dpf when treated with GsMTx4 there was a significant reduction in response with 0% of animals (n=4 DRG) expressing non-neuronal GCaMP6s responded to mechanical force and 25% of animals (n=4 DRG) expressing neuronal GCaMP6s responded to mechanical force (sox10 3dpf DMSO vs. GsMTx4: p=0.0110, neurod 3dpf DMSO vs. GsMTx4: p=0.0476 Fisher's exact test) (Fig 2C). These data support the hypothesis that DRG are responsive to mechanical forces and identify that *sox10*$^{+}$ cells are mechanosensitive, at least partially independent of neuronal activity.

Non-neuronal Ca^{2+} transients can be altered by manipulating piezo1

We next explored the potential molecular determinant of this mechanical component. The mature DRG is known to express mechanosensitive channels Piezo1 and Piezo2, however Piezo2 is restricted to neurons while Piezo1 is expressed in neurons and satellite glia in mice[31]. To investigate this in zebrafish, we utilized RNAscope to determine spatiotemporal distribution of *piezo1* RNA in animals expressing *Tg(sox10:meGFP)*. We found that 79% of DRG (n=24 DRG) at 3 dpf contained *piezo1* RNAscope puncta (Fig 2H).

To test if DRG contains functional Piezo1, we treated animals expressing *Tg(sox10:gal4+myl7); Tg(uas:GCaMP6s)* with Yoda1 and Jedi2, known Piezo1 specific agonists (Fig 2G-J). We found the average amount of Ca^{2+} activity per *sox10*$^{+}$ cell in a 1 hour timelapse in DMSO controls was 2.69±1.55 activity events, which was significantly less than the average 4.48±1.58 activity events or 4.58±2.54 activity events observed when treated with Yoda1 or Jedi2 respectively (DMSO n=52 cells, 17 DRG, Yoda1 n=33 cells, 9 DRG, Jedi2 n=79 cells, 18 DRG) (DMSO vs. Yoda1: p<0.0001 unpaired t test, DMSO vs. Jedi2: p<0.0001 unpaired t test) (Fig 2I-L). Furthermore, we repeated this assay treating with GsMTx4 to investigate whether inhibiting mechanosensitive ion channels reduces spontaneous Ca^{2+} activity. This treatment significantly reduced the average amount of Ca^{2+} activity per *sox10*$^{+}$ cells to an average of 2.05±1.36 Ca^{2+} events (n=44 cells) (DMSO vs GsMTx4: p=0.0342 unpaired t test) (Fig 2 I-L).

One possible explanation for an increase in Ca^{2+} activity in *sox10*$^{+}$ glia is that the *sox10*$^{+}$ glia are active in response to neuronal activity. To investigate whether the observed change in Ca^{2+} activity in *sox10*$^{+}$ cells was a consequence of altered neuronal activity, we treated animals expressing *Tg(neurod:gal4+myl7); Tg(uas:GCaMP6s)* with Piezo1 agonists and quantified the amount of Ca^{2+} activity per DRG neuron. We found following DMSO treatment that DRG neurons exhibited an average of 2.42±1.71 Ca^{2+} activity events per hour. When animals were treated with either Yoda1 or Jedi2, an average of 3.50±2.39 or 2.57±2.00 Ca^{2+} activity events per hour respectively could be detected. When animals were treated with GsMTx4, there was an observed 3.75±1.67 average number of Ca^{2+} activity events (DMSO n=33 neurons, Yoda1 n=8 neurons, Jedi2 n=35 neurons, GsMTx4 n=8 neurons) (Fig 2M). Overall, we found that Piezo1 agonists did not contribute to an increase in Ca^{2+} activity in the *neurod*$^{+}$ population. These data are most consistent with the hypothesis that *sox10*$^{+}$ glia are active in response to Piezo1 agonists independent of an increase in neuronal activity.

We demonstrated that DRG non-neuronal cells have distinct Ca^{2+} transients (Fig 1D-F) but the underlying mechanism of those transients is unknown. We therefore tested if subtypes of Ca^{2+} transients were differentially modulated by Piezo1. To investigate the role of Piezo1 in isolated and simultaneous Ca^{2+} events, we quantified the effect of Yoda1, Jedi2, GsMTx4, and DMSO treatment on these Ca^{2+} events. In DMSO-treated animals, *sox10*$^{+}$ cells displayed an average 0.46±0.78 isolated Ca^{2+} events. When treated with Yoda1 or Jedi2, *sox10*$^{+}$ cells displayed an average of 2.28±1.72 or an average of 1.31±1.22 isolated Ca^{2+} events respectively. We found that when treated with GsMTx4, *sox10*$^{+}$ cells displayed an average of 0.91±1.2 isolated Ca^{2+} events (DMSO n=24 cells, Yoda1 n=28 cells, Jedi2 n=59 cells, GsMTx4 n=23 cells) (Fig 3A-C). These results show that Piezo1 agonists significantly increased the amount of isolated activity (DMSO vs. Yoda1: p<0.0001, DMSO vs. Jedi2: p=0.0024 unpaired t tests), while mechanosensitive antagonists did not significantly decrease isolated activity (DMSO vs GsMTx4: p=0.1294 unpaired t test) (Fig 3C). In contrast, simultaneous Ca^{2+} events were not significantly different in Yoda1 or Jedi2-treated animals compared to controls (Fig 3D). In the case of mechanosensitive antagonists, animals displayed a significant decrease in the number of simultaneous activity events compared to DMSO control when treated with GsMTx4 (DMSO vs. GsMTx4: p=0.0003 unpaired t test). Lastly, we also quantified the number of Ca^{2+} microdomains following manipulations of Piezo1 in *Tg(sox10:gal4+myl7)* animals injected with

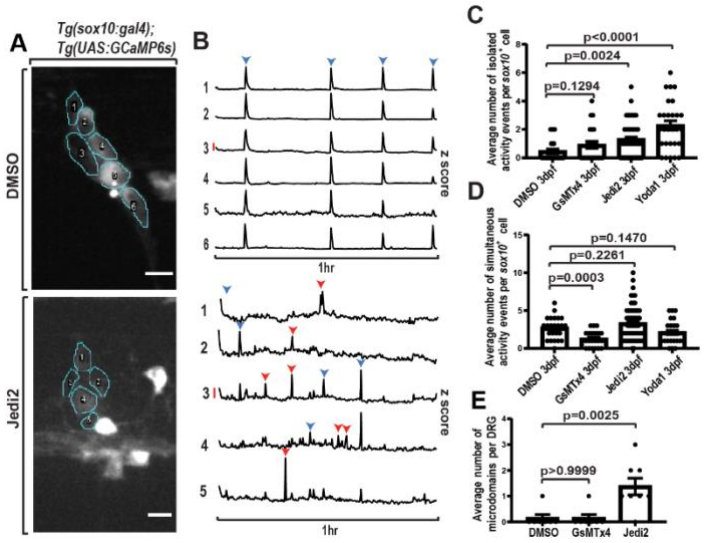

Figure 3: Piezo1 overactivation increases isolated calcium activity in DRG A) Confocal z-projection of DRG in 3 dpf animal expressing *Tg(sox10:gal4);Tg(uas:GCaMP6s)* and treated with either 2% DMSO or 40µM Jedi2. Individual cells are traced for ROIs and labeled with a number. B) Line graphs of the z score of the integrated density of fluorescence over a 1 hr period. Each numbered line graph corresponds to a numbered ROI. Red scale bar represents a z score of 2.58. Blue arrowheads note simultaneously active time points. Red arrowheads note isolated active time points. C) Quantification of the average number of isolated activity events per *sox10*$^+$ cell in 3 dpf animals expressing *Tg(sox10:gal4); Tg(uas:GCaMP6s)* that were treated with either 2% DMSO, 1µM GsMTx4, 100µM Yoda1, or 40µM Jedi2. D) Quantification of the average number of simultaneous activity events per *sox10*$^+$ cell in 3 dpf animals expressing *Tg(sox10:gal4); Tg(uas:GCaMP6s)* that were treated with either 2% DMSO, 1µM GsMTx4, 100µM Yoda1, or 40µM Jedi2. E) Quantification of the average number of microdomains per DRG in 3 dpf animals expressing *Tg(sox10:gal4); uas:GCaMP6s-caax* that were treated with either 2% DMSO, 1µM GsMTx4, or 40µM Jedi2 for 30 minutes prior to imaging. Scale bar is 10µm (A). Statistical tests: unpaired t test (C, D), one-way ANOVA followed and represented by post hoc dunnett test (E).

uas:GCaMP6s-caax. In DMSO-treated animals, *sox10*$^+$ cells displayed an average number of 0.14±0.38 Ca^{2+} microdomains. Animals treated with Jedi2 displayed an average number of 1.38±0.92 Ca^{2+} microdomains. When animals were treated with GsMTx4 we observed an average of 0.14±0.38 Ca^{2+} microdomains (DMSO n=7 DRG, Jedi2 n=8 DRG, GsMTx4 n=7 DRG) (Fig 3E). Similar to isolated activity, we found a significant increase in the average number of Ca^{2+} microdomains per DRG when animals were treated with a Piezo1 agonist (DMSO vs. Jedi2: p=0.0025 post hoc dunnett test) (Fig 3E). These additional findings suggest that Piezo1-mediated mechanical forces contribute to isolated Ca^{2+} activity events and Ca^{2+} microdomain events.

Altering Piezo1 has functional consequences to DRG development and function

The specific function of distinct Ca^{2+} transients is relatively unknown. We therefore used Piezo1 manipulations to test the potential functional consequence of disrupting distinct Ca^{2+} transients. We first hypothesized that Piezo1-sensitive isolated Ca^{2+} transients were important for the formation of synchronized glial networks. These glial networks form between 2-4 dpf (Figure 1I). Therefore, to first test this hypothesis, we treated animals expressing *Tg(sox10:gal4+myl7); Tg(uas:GCaMP6s); Tg(neurod:tagRFP)* with either DMSO, GsMTx4, or Jedi2 for 30 minutes daily at 2 and 3 dpf. We performed our Ca^{2+} imaging paradigm on these animals at 4 dpf and first assessed the amount of isolated and spontaneous Ca^{2+} activity following consecutive days of treatment. Following consecutive days treated with DMSO, *sox10*$^+$ cells showed an average of 2.06±1.85 simultaneous activity events and an average of 0.63±0.75 isolated activity events. Following treatment on consecutive days with Jedi2, *sox10*$^+$ cells showed an average of 1.56±1.19 simultaneous activity events and an average of 1.52±1.85 isolated activity events. Taken together these data confirm that following consecutive days of treatment, Jedi2 significantly increases the amount of isolated Ca^{2+} activity (DMSO vs. Jedi2: p=0.0132 post hoc dunnett test). Interestingly, after treatment with the broad-mechanosensitive antagonist, GsMTx4, on consecutive days in development, *sox10*$^+$ cells displayed an average of 0.86±0.56 simultaneous activity events and an average of 0.68±0.72 isolated activity events, significantly reducing the amount of simultaneous Ca^{2+} activity (DMSO vs. GsMTx4: p=0.0050 post hoc dunnett test) (DMSO n=32 cells, Jedi2 n=25 cells, GsMTx4 n=22 cells) (Fig 4D,E). To answer whether these changes ultimately impacted synchrony, we quantified the average percent of high correlation coefficients per cell following these treatment paradigms. We found that when treated with DMSO, *sox10*$^+$ cells had an average of 35.88±28.78% of high correlation coefficients. When treated with either GsMTx4 or Jedi2, *sox10*$^+$ cells had an average of 29.09±31.65% high correlation coefficients or an average of 24.48±27.16% high correlation coefficients respectively (DMSO n=32 cells, GsMTx4 n=22 cells, Jedi2 n=25 cells) (Fig 4F). There was no significant change in the average percent of high correlation coefficients when treated with Jedi2 or GsMTx4 and thereby inconsistent with the idea that Piezo1-sensitive isolated Ca^{2+} events or Ca^{2+} microdomains impact the formation of a presumptive glial network, at least as identified by synchronous activity.

In addition to the synchronous glial networks that we identify form by 4 dpf, it is also known that the DRG rapidly expands during this developmental time[44]. We, therefore, tested the hypothesis that Piezo1-sensitive events like isolated activity could be important for DRG expansion. To do this, we increased isolated activity via Piezo1 through Jedi2 or Yoda1 treatment and assessed the number of cells present in the DRG at 5 dpf. To assay both neuronal and glial expansion, we treated zebrafish expressing *Tg(neurod:tagRFP)* with Piezo1 agonists or a mechanosensitive antagonist for 30 minutes each day from 2-4 dpf, and then used immunohistochemistry against Sox10 to identify TagRFP$^+$ neurons and Sox10$^+$ non-neuronal cells at 5 dpf. Animals treated with DMSO on consecutive days displayed an average number of 3.85±1.05 *neurod*$^+$ cells and an average number of 5.09±1.33 Sox10$^+$ cells. When animals were treated with GsMTx4, DRG also contained an average of 4.18±1.22 *neurod*$^+$ cells and 4.91±0.99 Sox10$^+$ cells. However, treatment with Jedi2, resulted in DRG with an average of 2.23±0.81 *neurod*$^+$ cells and average number of 3.36±0.81 Sox10$^+$ cells (Fig 4I-J), showing a reduction in the amount of DRG cells (DMSO vs. Jedi2: p<0.0001 post hoc dunnett test) (DMSO n=53, GsMTx4 n=34 DRG, Jedi2 n=39 DRG). With treatment with

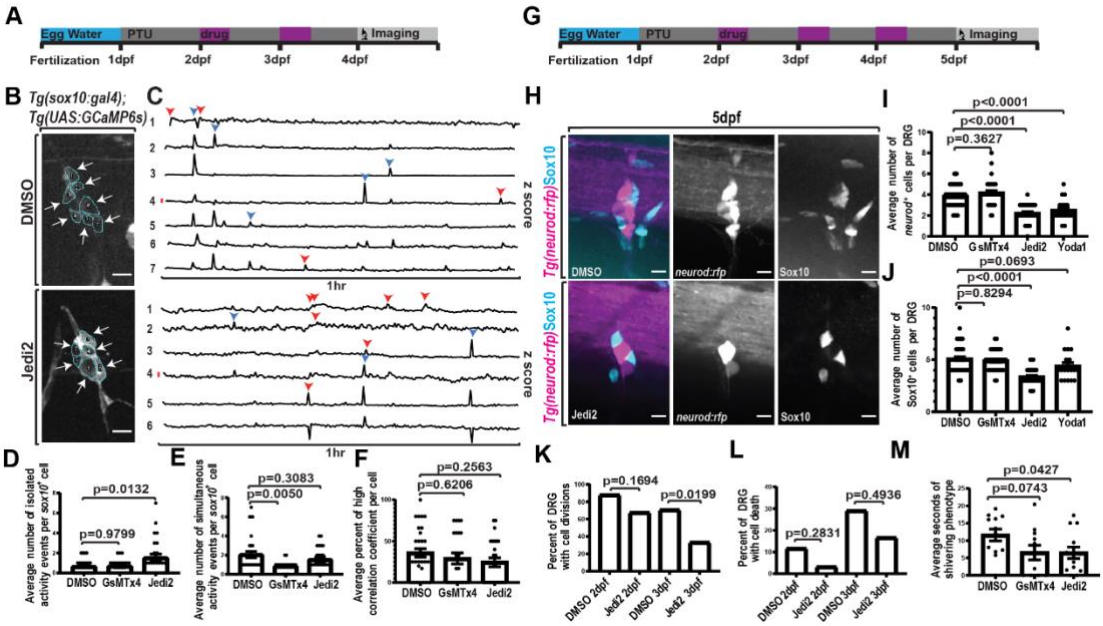

Figure 4: Increased isolated activity via Piezo1 decreases DRG cell divisions and reduces response to cold stimulus A) Timeline of experimental process where animals were treated with either 2% DMSO, 1µM GsMTx4, or 40µM Jedi2 for 30 minutes each day at 2 and 3 dpf. B) Confocal z-projection of DRG in animals expressing *Tg(sox10:gal4); Tg(uas:GCaMP6s)* following consecutive days of treatment with either DMSO or Jedi2. ROIs are traced individual cells labeled with a number. Arrows denote active cells. C) Line graphs of the z score of the integrated density of fluorescence over a 1 hr period. Numbers correlate with ROIs in (B). Red line signifies a z score of 2.58. Blue arrowheads note simultaneous active time points. Red arrowheads note isolated active time points. D-F) Quantification of the average number of isolated (D), simultaneous Ca^{2+} activity events per *sox10*$^{+}$ cells (E) or average percent of high correlation coefficient(F) per*sox10*$^{+}$ in 4 dpf animals expressing *Tg(sox10:gal4); Tg(uas:GCaMP6s)* that were treated at 2 and 3 dpf with DMSO, GsMTx4, or Jedi2. G) Timeline of experimental process where animals were treated with either 2% DMSO, 1µM GsMTx4, 100µM Yoda1, or 40µM Jedi2 for 30 minutes each day at 2-4 dpf. Animals were then fixed and processed for imaging at 5 dpf. H) Confocal z-projections of 5 dpf DRG in animals expressing *Tg(neurod:tagRFP)* and stained for Sox10. Magenta displays *Tg(neurod:tagRFP)*, and cyan displays Sox10. I-J) Quantification of the average number of *neurod*$^{+}$ (I) and Sox10 (J) cells in 5 dpf animals treated with either 2% DMSO, 1µM GsMTx4, 40µM Jedi2, or 100µM Yoda1 for 30 minutes each day from 2-4 dpf. K-L) Quantification of the percent of DRG with cell divisions (K) and/or cell deaths (L) in 24-hour time lapses of *Tg(sox10:meGFP); Tg(neurod:tagRFP)* animals treated either with 2% DMSO or 40µM Jedi2 from 2-3 dpf or 2-4 dpf. M) Quantification of the average duration (seconds) of shivering in of 5 dpf animals that were treated with 2% DMSO, 1µM GsMTx4, or 40µM Jedi2 for 30 min each day from 2-4 dpf. Scale bar is 10µm (B,H). Statistical tests: one-way ANOVA followed and represented by post hoc dunnett test (D, E, F, I, J), Fisher's exact: (K, L), unpaired t test: (M).

Yoda1, DRG (n=18 DRG) also displayed a significant reduction in DRG cells, with an average number of 2.50±1.04 *neurod*$^{+}$ cells (DMSO vs. Yoda1: p<0.0001, post hoc dunnett test). Taken together, these findings identify a potential consequence to altering Piezo1-sensitive isolated or microdomain Ca^{2+} transients.

It is possible that this decrease in cell abundance was caused by a decrease in cell divisions or from an increase in cell death. In order to understand the cause of the decrease in cell abundance, we assessed the number of cell divisions and cell death occurring following consecutive treatment with Piezo1 agonists. To do this, we treated animals expressing *Tg(sox10:meGFP)* from 2-4 dpf with Jedi2 or a DMSO control. We then utilized overnight time lapse imaging to assay cell divisions or cell death. When treated with DMSO at 2 dpf, 88.24% of DRG had cell divisions (n=17 DRG). At 3 dpf following DMSO treatment, cell division occurred in 70.83% of DRG (n=24 DRG). Following treatment of Jedi2 at 2 dpf, 67.74% of DRG had cell divisions (n=31 DRG). At 3 dpf following consecutive treatment with Jedi2, 33.33% of DRG had cell divisions (n=24 DRG) (Fig 4K). We found a significant decrease in the number of cell divisions following consecutive treatment of Jedi2 at 2 and 3 dpf (DMSO vs Jedi2 3dpf: p=0.0199 Fisher's exact test) (Fig 4K). However, we did not observe a significant change in the number of observed cell deaths (Fig 4L). The most likely explanation for this data is that the decrease in cell abundance in Piezo1-manipulated animals is from a reduction in cell divisions.

Lastly, we questioned whether this Piezo1-mediated decrease in cell abundance had functional consequences to the animal's physiology. To answer this question, we treated animals with Piezo1 agonists and mechanical-channel antagonists during development and then tested the animals response to sensory stimuli. We previously demonstrated that larval zebrafish DRG neurons are active after zebrafish larvae are submerged in 4℃ water[45,46]. This submersion causes a shivering phenotype that is at least partially dependent on intact DRG neurons and axons[45,46]. We treated animals with Jedi2 or GsMTx4 for 30 minutes each day from 2-4 dpf and then assayed sensory responses at 5 dpf. Following consecutive days of treatment, DMSO control treated animals had a shivering phenotype average duration of 11.60±5.9s. When treated on consecutive days with GsMTx4, animals had an average length of shivering of 6.55±6.97s. Following consecutive days of treatment with

Jedi2, animals had an average length of shivering of 6.47±6.01s. There was a significant decrease in the length of shivering following consecutive days of Jedi2 treatment suggesting that overactivation of Piezo1 during development impacts DRG response to noxious stimulus (DMSO vs Jedi2: p=0.0427 unpaired t test) (DMSO n=12 animals, GsMTx4 n=11 animals, Jedi2 n=13 animals) (Fig 4M).

DISCUSSION:

Activity of neural cells during development is well documented. This activity can be broadly categorized into evoked and spontaneous activity. In glia, spontaneous activity is further divided into subtypes characterized as whole cell and microdomain Ca^{2+} transients. However, the developmental, molecular and functional features of these glial transients merits more investigation. Here, we demonstrate that non-neuronal cells in the DRG exhibit distinct subtypes of spontaneous activity during early developmental times. We further reveal that distinct subtypes of Ca^{2+} transients are sensitive to manipulation of Piezo1. The functional consequence of disrupting such Piezo1-sensitive events is supported by data that shows cell abundance and sensory behavior is impacted by Piezo1-manipulations. Overall, we reveal developmental, molecular and functional characteristics of glial transients in the DRG.

Despite clear roles of neural activity in development and homeostasis of the nervous system in the animal, it is unclear when and which cells in the DRG are spontaneously active. It is well appreciated that cultured DRG neurons exhibit spontaneous activity[47,48]. Ca^{2+} reporters have also demonstrated that satellite glia demonstrate Ca^{2+} transients in culture[49,50]. These cultured satellite glia also exhibit synchronized Ca^{2+} transients. Recent work has also shown Ca^{2+} activity in the vertebrate DRG neurons *in vivo*[51,52]. However, such work was restricted to mature animals. Our work reveals that both DRG neurons and glia in the animal are active during the earliest stages of DRG construction. Even on the first day of genesis, DRG cells demonstrate Ca^{2+} transients. We also identify the molecular mechanisms that mediate some of these Ca^{2+} transients. What remains unknown is how these Ca^{2+} transients change as the animal approaches adulthood or in neuropathologies. These are important topics to study because we know altered activity of both glia and neurons has been implicated in neuropathologies. Further, in addition to the spontaneous Ca^{2+} transients we focus on, neurons in the DRG also are evoked by specific stimuli. How non-neuronal cells respond to evoked stimulation in the animal is almost entirely unknown.

By imaging GCaMP6s in *sox10*$^{+}$ cells and probing gap junction components, we reveal that synchronized cellular activity indicative of glial networks form within 3 days of DRG genesis. We know that glial networks are essential in the central nervous system for circuit formation, neuronal health, and signal transduction. However, glial networks in the peripheral nervous system are less understood. Because of this, whether glial networks exist in developing DRG was not known. Our work identifies that DRG glia are not synchronized initially, but by 4 days of DRG construction, become synchronized. One interesting aspect of this increased synchronization is that it occurs while the population is simultaneously expanding via cell divisions. Further investigation in additional PNS populations will provide an understanding if this is a unique process to the DRG, or if it is found in additional areas of the peripheral nervous system. It will also be important to probe the plasticity of the synchronized glial network and how it could be altered.

While most currently published research has focused on identifying molecules involved in synchronous activity of cells that make up neural circuits, we have identified a mechanism that contributes specifically to what we define as isolated activity within the DRG. We found that mechanobiology via Piezo1 contributes to an increase in isolated activity without altering simultaneous activity. Our findings provide insights into the importance of understanding mechanical forces on the cellular level during development. It is possible that these mechanical forces provide insight to satellite glia regarding whether or not proliferation is needed. For example, if the mechanical forces acting on a satellite glia are high, this may cause signaling via Piezo1 to halt or promote proliferation[29,35,53]. Alternatively, the ability to sense larger mechanical forces on the level of tissues may be important for DRG expansion. If this were true, an increase in mechanical forces may signal to the DRG that there is no room for further proliferation. One potential signaling cascade that may be involved in YAP/Taz. YAP/Taz is a well-known controller of cellular proliferation and has also been shown to modulate DRG development[13]. So, it is possible that over activating Piezo1 is altering localization of Yap/Taz[54]. Another area of research that would impact these ideas is the utility of Ca^{2+} microdomains observed in the DRG. If these microdomains are indicative of mechanical forces on the subcellular level, we may hypothesize either an increase or decrease in the amount of these microdomains which would further inform proliferative decisions in DRG glia. Further investigation into the mechanical forces acting on the microenvironment of the DRG needs to be completed.

Our findings highlight the importance of understanding the role of mechanical signals in PNS development and the function of distinct Ca^{2+} transients in that process.

Limitations of findings

We found a transition from an asynchronous population to a synchronous population during early DRG development. We attribute this transition to an increase in correlation coefficients between cells present in the DRG, which we hypothesize is a result from increased gap junction formation. But, this transition may also be partially explained by other processes. This work only investigates Ca^{2+} transients in the first 3 days of DRG genesis, so whether the observed synchrony remains through later stages of development is unknown and merits further study. We currently hypothesize that the decrease in cell proliferation is a result of Piezo1 overactivation. Whether Piezo1 controls proliferation only through isolated activity cannot be determined with our experiments. Our work also does not distinguish between cell-autonomous and non-autonomous roles of Piezo1 in satellite glia. Because of this, we cannot rule out the possibility that the observed phenotypes are a result of non-autonomous signaling. However, the *piezo1* expression in DRG cells and response to Piezo1 agonists suggests a cell-autonomous role. But it remains a possibility that over activating Piezo1 could result in

a change in a cell's ability to communicate unidentified signals to surrounding cells. If this is the case, then non-autonomous roles of Piezo1 could contribute to the reduction in cell abundance.

ACKNOWLEDGEMENTS:
We thank members of the Wingert, Patzke and Smith labs for helpful discussions. Thank you to David Lyons for sharing GCaMP6s transgenic zebrafish. We also thank 3i for fielding imaging related questions and Deborah Bang, Brittany Gervais and others for zebrafish housing and upkeep. This work was supported by The Garibaldi Family Endowment for Excellence in Adult Stem Cell Research (JPB), The Hiller Family and Garibaldi Family Fellowships in Stem Cell and Regenerative Biology (JPB), Michael and Elizabeth Gallagher Family (CJS), The University of Notre Dame (CJS), the SMART foundation (CJS), and the NIH (DP2NS117177)(CJS). The funders had no role in study design, data collection, analysis, decision to publish or preparation of the manuscript.

AUTHOR CONTRIBUTIONS STATEMENT:
JPB performed all the analysis and experimentation, wrote the paper and conceived the study. CJS wrote and edited the manuscript and supervised and funded the project.

COMPETING INTERESTS STATEMENT:
The authors declare no competing interests.

MATERIALS AND METHODS:

Experimental Model and subject details

Experimental procedures adhered to the NIH guide for the care and use of laboratory animals. All experiments were approved by the University of Notre Dame Institutional Animal Care and Use Committee (IACUC) (protocol 19-08-5464) which is guided by the United States Department of Argriculture, the Animal Welfare Act (USA) and the Assessment and Accreditation of Laboratory Animal Care International.

Animal Specimens. Danio rerio (zebrafish) were utilized in this study. The following stable strains were used: AB, *Tg(sox10:gal4+myl7:gfp)*[55], *Tg(uas:GCaMP6s)*[56], *Tg(neurod:gal4+myl7:gfp)*[57], *Tg(sox10:meGFP)*[58], *Tg(neurod:tagRFP)*[59], *Tg(ngn1:GFP)*[60]. All embryos were produced through pairwise matings and grown in 28ºC in constant darkness. At 24 hpf, zebrafish were exposed to PTU (0.0003%) to reduce pigmentation for intravital imaging. Age of animals was determined by hour post fertilization and stages of development[61].

Experimental Procedures

In vivo overnight imaging

Animals were anesthetized using veterinary grade 3-aminobenzoic acid ester (Tricaine) for mounting purposes only. Animals were then mounted laterally on their right side in glass-bottomed 35 mm petri dishes[44] and covered in 0.8% low melt agarose. For overnight time lapse imaging, a mixture of egg water and tricaine was added to the dish. Images were acquired on spinning disk confocal microscopes custom built by 3i technology (Denver, CO) that contains: Zeiss Axio Observer Z1 Advanced Mariana Microscope, X-cite 120LED White Light LED System, filter cubes for GFP and mRFP, a motorized X,Y stage, piezo Z stage, 20X Air (0.50 NA), 63X (1.15NA), 40X (1.1NA) objectives, CSU-W1 T2 Spinning Disk Confocal Head (50 µm) with 1X camera adapter, and an iXon3 1Kx1K EMCCD camera or Prime 95B back illuminated CMOS camera, dichroic mirrors for 446, 515, 561, 405, 488, 561,640 excitation, laser stack with 405 nm, 445 nm, 488 nm, 561 nm and 637 nm. Overnight time-lapse images were collected every 5 min for 24 hours capturing a 40µm z stack. Adobe Illustrator and ImageJ were used to process images. Only brightness and contrast were adjusted and enhanced for images represented in this study.

in vivo calcium imaging

Animals were anesthetized using veterinary grade 3-aminobenzoic acid ester (Tricaine) for mounting purposes only. Animals were then mounted laterally on their right side in glass-bottomed 35 mm petri dishes[44] and covered in 0.8% low melt agarose. For Ca^{2+} imaging, egg water was added to the dish with no Tricaine. Images were acquired on a spinning disk confocal microscope custom built by 3i technology (Denver, CO) microscopes. Ca^{2+} time-lapse imaging consisted of image collection every 15 seconds for 1 hour capturing a 40µM z stack. For imaging of Ca^{2+} microdomains, images were either taken every 5s for 10 minutes capturing a 20µm z stack (Fig 1) or taken every 200ms in a single plane (Fig 2). Adobe Illustrator and ImageJ were used to process images. Only brightness and contrast were adjusted and enhanced for images represented in this study.

Pharmacological treatments

For this study, we used chemical treatments of HMR1556 20µM (Sigma-Aldrich), Thapsigargin 10µM (Sigma-Aldrich), Apyrase 10U (Sigma-Aldirch), Carbenoxolone 100µM (Tocris), GsMTx4 1µM (Tocris), Yoda1 100µM (Tocris), and Jedi2 40µM (Tocris). HMR1556 was stored at 10mM concentration at -20ºC. Thapsigargin was stored at 10mM concentration at -20ºC. Apyrase was stored at 100U in -20ºC. GsMTx4 was stored at 1mM at -20ºC. Yoda1 was stored at 10mM at 4ºC in 100% DMSO. Jedi2 was stored at 10mM at 4ºC. All treatments were done in 2% DMSO. Control groups were treated with 2% DMSO throughout.

Consecutive Treatments of Pharmacological treatments

For consecutive days of treatment with pharmacological treatments animals were bathed in a mixture of either 40µM Jedi2, 1µM GsMTx4, or 100µM Yoda1 in egg water with 2% DMSO for 30 minutes each day. For Fig 4A-4F only the 40µM Jedi2 and 1µM GsMTx4 mixtures or a 2% DMSO egg water control were used. These treatments occurred at 2dpf and 3dpf. For Fig 4G-4J mixtures of 40µM Jedi2, 1µM GsMTx4, and 100µM Yoda1 mixtures or a 2% DMSO egg water control were used. These treatments occurred at 2dpf, 3dpf, and 4dpf. For Fig 4K-4L animals were treated with either 40µM Jedi2 or 2% DMSO egg water at 2 and 3dpf. For Fig 4M animals were treated with 40µM Jedi2, 1µM GsMTx4, or 2% DMSO egg water at 2dpf, 3dpf, and 4dpf.

Whole-mount immunohistochemistry

The primary antibody used to identify formation of gap junctions was Cxn43 (1:500; Cell Signaling Technology) (Fig 1K). The primary antibody used to identify cells expressing *Tg(sox10:meGFP)* was GFP (1:500; Aves) (Fig 2G) following the listed RNAscope protocol. The primary antibody used to identify non-neuronal cells present in the DRG was Sox10 (1:1000, Sarah Kucenas Lab) (Fig 4H). The secondary antibody used in both of these experiments was Alexa Fluor 488 (1:500; Invitrogen). Animals were fixed in 4% PFA in PBSt (PBS, 0.1% TritonX-100) at 2dpf (Fig 2G) or 5dpf (Fig 4H). Animals were then washed for 5 minutes in a series of PBSt, DWt (dH_2O, 0.1% TritonX-100), and acetone. Following these washes, animals were placed in acetone at -20ºC for 10 minutes. This was then followed by 3 washes of PBSt for 5 minutes each. Animals were then placed in 5% goat serum in PBSt for a 1 hour incubation period. Animals were then incubated in 5% goat serum in PBSt with primary antibody for 1 hour at room temperature followed by an overnight incubation at 4ºC. This was followed by 3 consecutive 30 minutes washes of PBSt and one 1 hour wash in PBSt. Animals were then placed in 5% goat serum in PBSt with the secondary antibody for 1 hour at room temperature followed by an overnight incubation at 4ºC. This was then followed by 3 consecutive 1 hour washes of PBSt. Animals were then stored in 50% glycerol 50% PBS at 4ºC until imaging.

Whole-mount RNAscope

Animals expressing *Tg(sox10:meGFP)* were fixed at 2dpf with 4%PFA in PBS for 30 minutes. Following fixation animals were placed in new eppendorf tubes and washed with 25%, 50%, 100% methanol for 10 minutes each. Animals were then kept in 100% methanol at -20ºC overnight. This was followed by a 5 minute

wash of 50% methanol in PBStw (PBS, 0.1% Tween-20) and an additional 5 minute wash of 25% methanol in PBStw. Liquid was removed from the eppendorf tubes and the animals were air dried for 30 minutes. This was followed by two 5 minute washes with PBStw. Animals were permeabilized with 10ug/mL proteinase K in PBStw at room temperature for 6 minutes. This was then followed by 4 consecutive 10 minute washes of PBStw. Following removal of PBStw, 2 drops of ACD probes targeting *piezo1* were then added to the sample, which was then incubated at 40ºC for 15 hours (1:50, 80uL, C1, ACD). After this incubation period animals were then washed with SSCtw (5X saline-sodium citrate buffer, 0.1% Tween-20) for 10 minutes at room temperature twice. An additional fixation was then done in 4% PFA in PBS at room temperature for 10 minutes. Animals were again transferred to a new eppendorf tube and washed 3 times in SSCtw. Animals were then incubated in a series of 2 drops Amp1 at 40ºC for 30 minutes, 2 drops Amp2 at 40ºC for 30 minutes, 2 drops Amp3 at 40ºC for 15 minutes, 2 drops HRP-C1 at 40ºC for 30 minutes, opal fluorophore 650 (1:500) in PBStw at 40ºC for 30 minutes, and 2 drops of Multiplex FLv2 HRP blocker at 40ºC for 30 minutes. Between each of these incubation periods animals were washed twice with SSCtw. Following this protocol, animals were then processed following the Whole-mount immunohistochemistry protocol to target GFP.

Animal behavior in cold stimulus

Animals were treated at 2, 3, and 4 dpf with 1μM GsMTx4 in 2% DMSO, 40μM Jedi2 in 2% DMSO, or 2% DMSO in egg water for 30 minutes each day. Aside from this treatment protocol, animals were raised under normal procedures in 28ºC egg water. Each animal was then taken at 5dpf and placed in 4℃ egg water for 30 seconds. Video recordings were recorded with 40ms exposure to bright field white light. The initial 3 seconds of the movies were not quantified to allow the animal to be placed into the stimulus and for any adjustments to occur. The duration of the shivering was quantified per second starting from the initial shivering phenotype to the cold water stimulus until there was at least 1 second of no shivering.

Mechanical compression assay

To apply mechanical force to the DRG, we dorsally mounted animals in 0.8% low melt agarose and placed them on the stage of a spinning disk confocal. On either side of the stage two vertical stainless steel rods were mounted onto the air table. A horizontal rod was mounted above the stage with a micromanipulator attached. A glass needle filled with dextran was mounted in the micromanipulator above the animals with the needle pointing toward the animal. Prior to bringing into contact with the animal, the needle was calibrated in the X and Y positions in relation to the middle of the imaging window. The needle was slowly brought into contact with the skin of the animals and was then tapped to apply pressure to the DRG and surrounding tissue. To understand if DRG were active in response to the mechanical forces, we quantified GCaMP6s transients as previously described.

Microinjections

In order to label cell membranes with GCaMP6s, animals expressing *Tg(sox10:gal4+myl7:GFP)* were injected with *uas:GCaMP6s-caax* at the single cell stage. Injection mixes consisted of 12ng/uL *uas:GCaMP6s-caax*, 25ng/uL *tol2* (transposase), and phenol red (visualization). Animals were screened for expression of *uas:GCaMP6s-caax* and imaged for experiments.

Quantifications and Statistical Tests:

Quantification of GCaMP6s transients

Before quantifying changes in GCaMP6s intensity, we corrected for motion drift by utilizing the Template Matching plugin in ImageJ. We then traced individual cells in the DRG to create Regions of Interest (ROI). The integrated density of fluorescence was quantified at every time point for each ROI. We then quantified the z score for each timepoint for each ROI. Timepoints with a z score of 2.58 or greater were considered active timepoints. This process was used to create activity profiles for each ROI in a given DRG. The average number of active timepoints was calculated and compared to controls via t tests to determine significance.

Quantification of GCaMP6s transients in pilot screen

The number of GCaMP6s transients in the pilot screen were quantified in ImageJ. The number of visual changes in GCaMP6s intensity were quantified for each movie. These quantifications were done per whole DRG identified in the imaging window.

Generation of line graphs

Line graphs were generated using the data obtained from the quantification of GCaMP6s transients. Each cell in the DRG had GCaMP6s transients quantified. The X axis of the line graph is the 1 hr period and the Y axis is the Z score. Line graphs were generated in Prism.

Generation of Heatmaps

Heatmaps were generated in Prism. Each row of the heatmap corresponds to an individual cell's GCaMP6s transience during the 1hr of imaging. Blue colors indicate low z scores and yellow colors indicate high z scores (>2.58).

Quantification of Correlation Coefficients

Activity profiles from individual cells were converted to a binary system. Active points where the z score was greater than 2.58 were listed as 1 and inactive time points where the z score was less than 2.58 were listed as 0. These binary activity profiles were then used to quantify the correlation between individual ROIs found in the same DRG; we utilized the cor() function in R to complete this analysis. The results were then used to create a correlation table in R. These functions were part of the Hmisc package in R. Correlation coefficients greater than 0.5 were considered high correlation coefficients. The percent of high correlation coefficients were then quantified per cell and compared with controls via t tests to determine significance.

Quantification of IHC

All quantifications of IHC were completed in ImageJ. The number of Cxn43 puncta that coincided with *sox10:megfp* expression were quantified per DRG (Fig 1K,L). The number of DRG that contained *piezo1* within the stained GFP expressed was quantified (Fig 2G,H). The number of Sox10+ cells were quantified per DRG (Fig 4H,I).

Quantification of Mechanical Compression Assay

Response to mechanical compression was quantified in ImageJ. DRG were traced and the integrated density of fluorescence was quantified at each time point. To attempt quantifying only time points in the same z position, the beginning and end time points quantified were in the same z position that were not manually being changed using the microscope. Due to the nature of this experiment, tissue compression would still alter the z position of the DRG being quantified. To further account for this alteration, the change in integrated density of fluorescence was quantified by subtracting the initial time point from each time point being analyzed ($\Delta f = f - fi$). This value was then divided by the time point being analyzed ($\Delta f/f$). Large increases in this value following tissue compression were then scored as active responses to mechanical compression. Little to no change in this value following mechanical compression were scored as not active in response to tissue compression.

Statistical analysis

Statistical analysis was completed with Prism. No statistical methods were used to predetermine sample sizes but sample sizes are similar to previous publications. Statistical tests were completed with biological replicates, not technical replicates. No data points were excluded from the analysis. Healthy animals were randomly selected for all experiments. Each experiment was repeated at least with similar results. All data collected and analyzed are presented in the study.

Software

Slidebook, Prism, ImageJ, R, and Adobe Illustrator were used to acquire, analyze and compile figures.

DATA AVAILABILITY:

All data collected for this study are included in the figures and supplementary material.

REFERENCES:

1. Triplett MA, Avitan L, Goodhill GJ. Emergence of spontaneous assembly activity in developing neural networks without afferent input. PLoS Comput Biol. 2018;14: 1–22. doi:10.1371/journal.pcbi.1006421
2. Pietri T, Romano SA, Pérez-Schuster V, Boulanger-Weill J, Candat V, Sumbre G. The Emergence of the Spatial Structure of Tectal Spontaneous Activity Is Independent of Visual Inputs. Cell Rep. 2017;19: 939–948. doi:10.1016/j.celrep.2017.04.015
3. Avitan L, Pujic Z, Mo J, Amor R, Scott EK, Goodhill GJ, et al. Spontaneous Activity in the Zebrafish Tectum Reorganizes over Development and Is Influenced by Article Spontaneous Activity in the Zebrafish Tectum Reorganizes over Development and Is Influenced by Visual Experience. 2017; 2407–2419. doi:10.1016/j.cub.2017.06.056
4. Ma Z, Stork T, Bergles DE, Freeman MR. Neuromodulators signal through astrocytes to alter neural circuit activity and behaviour. Nature. 2016;539: 428–432. doi:10.1038/nature20145
5. Sasaki T, Ishikawa T, Abe R, Nakayama R, Asada A, Matsuki N, et al. Astrocyte calcium signalling orchestrates neuronal synchronization in organotypic hippocampal slices. J Physiol. 2014;592: 2771–2783. doi:10.1113/jphysiol.2014.272864
6. Stobart JL, Ferrari KD, Barrett MJP, Stobart MJ, Looser ZJ, Saab AS, et al. Long-term in vivo calcium imaging of astrocytes reveals distinct cellular compartment responses to sensory stimulation. Cereb Cortex. 2018;28: 184–198. doi:10.1093/cercor/bhw366
7. Kuijlaars J, Oyelami T, Diels A, Rohrbacher J, Versweyveld S, Meneghello G, et al. Sustained synchronized neuronal network activity in a human astrocyte co-culture system. Sci Rep. 2016;6: 1–14. doi:10.1038/srep36529
8. Ma Z, Freeman MR. Trpml-mediated astrocyte microdomain ca2+ transients regulate astrocyte-tracheal interactions. Elife. 2020;9: 1–18. doi:10.7554/ELIFE.58952
9. Rui Y, Pollitt SL, Myers KR, Feng Y, Zheng JQ. Spontaneous local calcium transients regulate oligodendrocyte development in culture through store-operated ca2+ entry and release. eNeuro. 2020;7: 1–16. doi:10.1523/ENEURO.0347-19.2020
10. Baraban M, Koudelka S, Lyons DA. Ca 2+ activity signatures of myelin sheath formation and growth in vivo. Nat Neurosci. 2018;21: 19–25. doi:10.1038/s41593-017-0040-x
11. Hösli L, Binini N, Ferrari KD, Thieren L, Looser ZJ, Zuend M, et al. Decoupling astrocytes in adult mice impairs synaptic plasticity and spatial learning. Cell Rep. 2022;38. doi:10.1016/j.celrep.2022.110484
12. Weiss S, Clamon LC, Manoim JE, Ormerod KG, Parnas M, Littleton JT. Glial ER and GAP junction mediated Ca2+ waves are crucial to maintain normal brain excitability. Glia. 2022;70: 123–144. doi:10.1002/glia.24092
13. Serinagaoglu Y, Paré J, Giovannini M, Cao X. Nf2-Yap signaling controls the expansion of DRG progenitors and glia during DRG development. Dev Biol. 2015;398: 97–109. doi:10.1016/j.ydbio.2014.11.017
14. Coronas V, Terrié E, Déliot N, Arnault P, Constantin B. Calcium Channels in Adult Brain Neural Stem Cells and in Glioblastoma Stem Cells. Front Cell Neurosci. 2020;14: 1–22. doi:10.3389/fncel.2020.600018
15. Venkatesh HS, Morishita W, Geraghty AC, Silverbush D, Gillespie SM, Arzt M, et al. Electrical and synaptic integration of glioma into neural circuits. Nature. 2019;573: 539–545. doi:10.1038/s41586-019-1563-y
16. Chen X, Wanggou S, Bodalia A, Zhu M, Dong W, Fan JJ, et al. A Feedforward Mechanism Mediated by Mechanosensitive Ion Channel PIEZO1 and Tissue Mechanics Promotes Glioma Aggression. Neuron. 2018;100: 799-815.e7. doi:10.1016/j.neuron.2018.09.046
17. Armstrong DM. Glutamate Receptor Subtypes Mediate Excitatory of Dopamine Neurons in Midbrain Slices Synaptic Currents. 1991; 3–4.
18. Cheramy A, Leviel V, Glowinski J. Dendritic release of dopamine in the substantia nigra. 1981;289: 537–542.
19. Micu I, Jiang Q, Coderre E, Ridsdale A, Zhang L, Woulfe J, et al. NMDA receptors mediate calcium accumulation in myelin during chemical ischaemia.

Nature. 2006;439: 988–992. doi:10.1038/nature04474
20. Káradóttir R, Cavelier P, Bergersen LH, Attwell D. NMDA receptors are expressed in oligodendrocytes and activated in ischaemia. Nature. 2005;438: 1162–1166. doi:10.1038/nature04302
21. Rose CR, Felix L, Zeug A, Dietrich D, Reiner A, Henneberger C, et al. Astroglial Glutamate Signaling and Uptake in the Hippocampus. 2018;10: 1–20. doi:10.3389/fnmol.2017.00451
22. Gonzalez A, Almeida A, Bolaños JP. Astrocyte NMDA receptors ' activity sustains neuronal survival through a Cdk5 – Nrf2 pathway. 2015; 1877–1889. doi:10.1038/cdd.2015.49
23. Bowser DN, Khakh BS. ATP Excites Interneurons and Astrocytes to Increase Synaptic Inhibition in Neuronal Networks. 2004;24: 8606–8620. doi:10.1523/JNEUROSCI.2660-04.2004
24. Zhang J, Wang H, Ye C, Ge W, Chen Y, Jiang Z, et al. ATP Released by Astrocytes Mediates Heterosynaptic Suppression. 2003;40: 971–982.
25. Puerto A, Wandosell F, Garrido JJ. Neuronal and glial purinergic receptors functions in neuron development and brain disease. 2013;7: 1–15. doi:10.3389/fncel.2013.00197
26. Koser DE, Thompson AJ, Foster SK, Dwivedy A, Pillai EK, Sheridan GK, et al. Mechanosensing is critical for axon growth in the developing brain. Nat Neurosci. 2016;19: 1592–1598. doi:10.1038/nn.4394
27. Espinosa-Hoyos D, Burstein SR, Cha J, Jain T, Nijsure M, Jagielska A, et al. Mechanosensitivity of Human Oligodendrocytes. Front Cell Neurosci. 2020;14: 1–15. doi:10.3389/fncel.2020.00222
28. Song Y, Li D, Farrelly O, Miles L, Li F, Kim SE, et al. The Mechanosensitive Ion Channel Piezo Inhibits Axon Regeneration. Neuron. 2019;102: 373-389.e6. doi:10.1016/j.neuron.2019.01.050
29. Pathak MM, Nourse JL, Tran T, Hwe J, Arulmoli J, Le DTT, et al. Stretch-activated ion channel Piezo1 directs lineage choice in human neural stem cells. Proc Natl Acad Sci U S A. 2014;111: 16148–16153. doi:10.1073/pnas.1409802111
30. Hill RZ, Loud MC, Dubin AE, Peet B, Patapoutian A. PIEZO1 transduces mechanical itch in mice. Nature. 2022;607: 104–110. doi:10.1038/s41586-022-04860-5
31. Wang J, La JH, Hamill OP. PIEZO1 is selectively expressed in small diameter mouse DRG neurons distinct from neurons strongly expressing TRPV1. Front Mol Neurosci. 2019;12: 1–15. doi:10.3389/fnmol.2019.00178
32. Abdo H, Calvo-Enrique L, Lopez JM, Song J, Zhang MD, Usoskin D, et al. Specialized cutaneous schwann cells initiate pain sensation. Science (80-). 2019;365: 695–699. doi:10.1126/science.aax6452
33. Ackerman SD, Perez-Catalan NA, Freeman MR, Doe CQ. Astrocytes close a motor circuit critical period. Nature. 2021;592: 414–420. doi:10.1038/s41586-021-03441-2
34. Shigetomi E, Tong X, Kwan KY, Corey DP, Khakh BS. TRPA1 channels regulate astrocyte resting calcium and inhibitory synapse efficacy through GAT-3. Nat Neurosci. 2012;15: 70–80. doi:10.1038/nn.3000
35. Rammensee S, Kang MS, Georgiou K, Kumar S, Schaffer D V. Dynamics of Mechanosensitive Neural Stem Cell Differentiation. Stem Cells. 2017;35: 497–506. doi:10.1002/stem.2489
36. Marinval N, Chew SY. Mechanotransduction assays for neural regeneration strategies: A focus on glial cells. APL Bioeng. 2021;5. doi:10.1063/5.0037814
37. Hughes AN, Appel B. Oligodendrocytes express synaptic proteins that modulate myelin sheath formation. Nat Commun. 2019;10: 1–15. doi:10.1038/s41467-019-12059-y
38. Hanani M, Spray DC. Emerging importance of satellite glia in nervous system function and dysfunction. Nat Rev Neurosci. 2020;21: 485–498. doi:10.1038/s41583-020-0333-z
39. Huang T, Belzer V, Hanani M. Gap junctions in dorsal root ganglia : Possible contribution to visceral pain. Eur J Pain. 2010;14: 49.e1-49.e11. doi:10.1016/j.ejpain.2009.02.005
40. Huang LYM, Gu Y, Chen Y. Communication between neuronal somata and satellite glial cells in sensory ganglia. Glia. 2013;61: 1571–1581. doi:10.1002/glia.22541
41. Retamal MA, Riquelme MA, Stehberg J, Alcayaga J. Connexin43 hemichannels in satellite glial cells, can they influence sensory neuron activity? Front Mol Neurosci. 2017;10: 1–9. doi:10.3389/fnmol.2017.00374
42. Komiya H, Shimizu K, Ishii K, Kudo H, Okamura T, Kanno K, et al. Connexin 43 expression in satellite glial cells contributes to ectopic tooth-pulp pain. J Oral Sci. 2018;60: 493–499. doi:10.2334/josnusd.17-0452
43. Ohara PT, Vit JP, Bhargava A, Jasmin L. Evidence for a role of connexin 43 in trigeminal pain using RNA interference in vivo. J Neurophysiol. 2008;100: 3064–3073. doi:10.1152/jn.90722.2008
44. Nichols EL, Green LA, Smith CJ. Ensheathing cells utilize dynamic tiling of neuronal somas in development and injury as early as neuronal differentiation. Neural Dev. 2018;13: 19. doi:10.1186/s13064-018-0115-8
45. Kikel-Coury NL, Green LA, Nichols EL, Zellmer AM, Pai S, Hedlund SA, et al. Pioneer axons utilize a Dcc signaling-mediated invasion brake to precisely complete their pathfinding odyssey. J Neurosci. 2021;41: 6617–6636. doi:10.1523/JNEUROSCI.0212-21.2021
46. Nichols EL, Smith CJ. Pioneer axons employ Cajal's battering ram to enter the spinal cord. Nat Commun. 2019;10. doi:10.1038/s41467-019-08421-9
47. Chen Y, Huang LYM. A simple and fast method to image calcium activity of neurons from intact dorsal root ganglia using fluorescent chemical Ca2+ indicators. Mol Pain. 2017;13: 1–9. doi:10.1177/1744806917748051
48. Teichert RW, Smith NJ, Raghuraman S, Yoshikami D, Light AR, Olivera BM. Functional profiling of neurons through cellular neuropharmacology. Proc Natl Acad Sci U S A. 2012;109: 1388–1395. doi:10.1073/pnas.1118833109
49. Suadicani SO, Cherkas PS, Zuckerman J, Smith DN, Spray DC, Hanani M. Bidirectional calcium signaling

between satellite glial cells and neurons in cultured mouse trigeminal ganglia. Neuron Glia Biol. 2010;6: 43–51. doi:10.1017/S1740925X09990408

50. Zhang X, Chen Y, Wang C, Huang LYM. Neuronal somatic ATP release triggers neuron-satellite glial cell communication in dorsal root ganglia. Proc Natl Acad Sci U S A. 2007;104: 9864–9869. doi:10.1073/pnas.0611048104
51. Chen C, Zhang J, Sun L, Zhang Y, Gan WB, Tang P, et al. Long-term imaging of dorsal root ganglia in awake behaving mice. Nat Commun. 2019;10: 1–11. doi:10.1038/s41467-019-11158-0
52. Chisholm KI, Khovanov N, Lopes DM, La Russa F, McMahon SB. Large scale in vivo recording of sensory neuron activity with GCaMP6. eNeuro. 2018;5: 1–14. doi:10.1523/ENEURO.0417-17.2018
53. Segel M, Neumann B, Hill MFE, Weber IP, Viscomi C, Zhao C, et al. Niche stiffness underlies the ageing of central nervous system progenitor cells. Nature. 2019;573: 130–134. doi:10.1038/s41586-019-1484-9
54. Dasgupta I, McCollum D. Control of cellular responses to mechanical cues through YAP/TAZ regulation. J Biol Chem. 2019;294: 17693–17706. doi:10.1074/jbc.REV119.007963
55. Hines JH, Ravanelli AM, Schwindt R, Scott EK, Appel B. Neuronal activity biases axon selection for myelination in vivo. Nat Neurosci. 2015;18: 683–689. doi:10.1038/nn.3992
56. Thiele TR, Donovan JC, Baier H. Descending Control of Swim Posture by a Midbrain Nucleus in Zebrafish. Neuron. 2014;83: 679–691. doi:10.1016/j.neuron.2014.04.018
57. Nichols EL, Smith CJ. Synaptic-like Vesicles Facilitate Pioneer Axon Invasion. Curr Biol. 2019;29: 2652-2664.e4. doi:10.1016/j.cub.2019.06.078
58. Kirby BB, Takada N, Latimer AJ, Shin J, Carney TJ, Kelsh RN, et al. In vivo time-lapse imaging shows dynamic oligodendrocyte progenitor behavior during zebrafish development. Nat Neurosci. 2006;9: 1506–1511. doi:10.1038/nn1803
59. McGraw HF, Snelson CD, Prendergast A, Suli A, Raible DW. Postembryonic neuronal addition in Zebrafish dorsal root ganglia is regulated by Notch signaling. Neural Dev. 2012;7: 1–13. doi:10.1186/1749-8104-7-23
60. McGraw HF, Nechiporuk A, Raible DW. Zebrafish dorsal root ganglia neural precursor cells adopt a glial fate in the absence of neurogenin1. J Neurosci. 2008;28: 12558–12569. doi:10.1523/JNEUROSCI.2079-08.2008
61. Kimmel CB, Ballard WW, Kimmel SR, Ullmann B, Schilling TF. Stages of embryonic development of the zebrafish. Dev Dyn. 1995;203: 253–310. doi:10.1002/aja.1002030302

SUPPLEMENTAL FIGURES

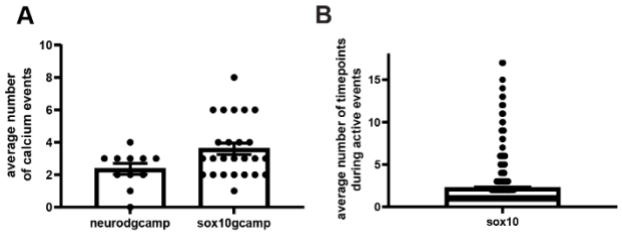

Supplemental Figure 1: DRG cells are spontaneously active A) Quantification of the average number of calcium events per *neurod*$^{+}$ cell or per *sox10*$^{+}$ cell in 3dpf animals expressing either *Tg(neurod:gal4+myl7); Tg(uas:GCaMP6s)* or *Tg(sox10:gal4+myl7); Tg(uas:GCaMP6s)*. B) Quantification of the average numer of timepoints during active events per *sox10*$^{+}$ cells in animals expressing *Tg(sox10:gal4+myl7); Tg(uas:GCaMP6s)*.

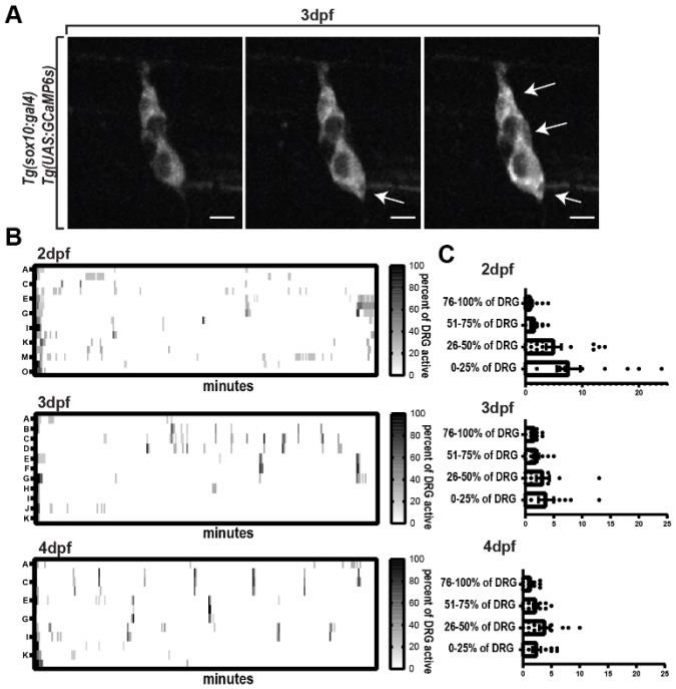

Supplemental Figure 2: Percent of active DRG cells increase during development A) Confocal z-projection of DRG in 3dpf animals expressing *Tg(sox10:gal4); Tg(uas:GCaMP6s).* Arrows note active cells and demonstrate different percentages of active DRG. B) Heatmaps of the percent of cells in the DRG active during a 1 hour period at 2, 3, and 4dpf. Darker gradient indicates a higher percent of cells active. C) Quantification of the number of active events with 0-25%, 26-50%, 51-75%, or 76-100% of DRG cells active at the same time point at 2, 3, and 4dpf.